ACS APPLIED MATERIALS & INTERFACES

Research Article

Cite This: ACS Appl. Mater. Interfaces 2019, 11, 40944−40950

www.acsami.org

Revealing Lectin−Sugar Interactions with a Single Au@Ag Nanocube

Jingjing Shen,[†] Lei Zhang,[*,†] Li Liu,[†] Bin Wang,[†] Jieqiong Bai,[†] Chao Shen,[†] Yu Chen,[†] Quli Fan,[*,†] Shufen Chen,[†] Weibing Wu,[*,‡] Xiaomiao Feng,[†] Lianhui Wang,[†] and Wei Huang[*,†,§]

[†]Key Laboratory for Organic Electronics and Information Displays & Institute of Advanced Materials (IAM), National Synergistic Innovation Center for Advanced Materials (SICAM), Nanjing University of Posts & Telecommunications, 9 Wenyuan Road, Nanjing 210023, China

[‡]Jiangsu Provincial Key Lab of Pulp & Paper Science & Technology, Nanjing Forestry University, Nanjing 210037, P. R. China

[§]Shaanxi Institute of Flexible Electronics (SIFE), Northwestern Polytechnical University (NPU), Xi'an 710072, China

Supporting Information

ABSTRACT: An individual nanoparticle-based plasmonic nanotechnology was used for real-time monitoring of lectin−sugar interactions, which could be designed as novel plasmonic nanobiosensors for the detection of trace concanavalin A (ConA) with high sensitivity and selectivity. The localized surface plasmon resonance (LSPR) spectra of Au@Ag nanocubes (NCs) are linearly shifted to a long wavelength with an increasing concentration of ConA. In fact, each Au@Ag NC can act as a nanobiosensor for the quantified detection of trace ConA, which enables the miniaturization of the biosensor system to nanoscale. Furthermore, the results demonstrated the perfect biosensing ability with the dual channel of dark-field microscopy images and LSPR spectra. We expect that this nanobiosensor system can provide an alternative important method for monitoring the specific binding of lectin−sugar at a single nanoparticle surface.

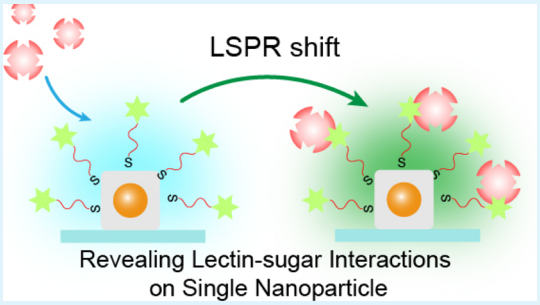

KEYWORDS: *plasmonics, nanobiosensor, lectin−sugar interactions, ConA, single nanoparticle*

1. INTRODUCTION

Glycosylation is one of the most important post-translational modifications in eukaryotic organisms, which is widely present on the cell membrane surface. Carbohydrates and lectin−sugar interactions are widespread and exist in all living organisms, governing a wide spectrum of pivotal biological and pathological events including cell−cell recognition, signal transduction, autoimmune stimulation, tumor metastasis, and so forth.[1−5] Trace glycan analysis in the different courses of diseases and related lectin−sugar interactions has drawn most researchers' attention recently.[6,7] For directly observing this process in vitro or in vivo, there are critical needs for developing effective new glycotechnology biosensors that are sensitive, rapid, simple, and more smaller in size which could be used for the real-time evaluation of binding mechanisms.[8] Plasmonics on a single nanoparticle, which usually depended on the coupling effect between adjacent plasmonic nanoparticles and inorganic compounds surrounding the nanoparticle, had offered a hopeful method for the trace analysis of target molecules by using a nanoscale sensing system, such as H_2S, NADH, Cu^{2+}, and so forth.[9−14] The plasmon resonance energy transfer effect could also be used for the fabrication of sensing chips for probing trace heavy metal ions[15−17] or the direct observation of chemical reactions.[18−21] These reports had made a great breakthrough in biosensor size down to nanometer scale. Besides, individual plasmonic nanoparticle localized surface plasmon resonance (LSPR) scattering spectra exhibited great dependence with the reflective index (RI) of the microenvironment around nanoparticles, which could be employed for developing novel plasmonic nanobiosensors in trace biomacromolecule analysis.[22−27]

Silver nanocubes (NCs), as two-dimensional plasmonic nanostructures, with well-defined and controllable shapes, have attracted intensive attention in the last decade because of their unique shape-dependent optical properties. However, traditional synthesis methods of Ag NCs need harsh reaction conditions with great difficulty in controlling the size and shape. Seed-mediated growth methods of monodispersed Au@Ag NCs use gold nanoparticles as seeds which could easily control the thickness of the Ag shell and adjust its LSPR scattering spectra. It was reported[28] that Au@Ag NCs with a silver medium layer of more thick surface showed plasmonic characters similar with those of Ag NCs. Compared with AuNPs, AuNCs, or AgNCs,[29−31] Au@Ag NCs were more sensitive, stable, suitable for long-term preservation, and used in biosensors.[32−34] In addition, these were used as near-field

Received: August 27, 2019
Accepted: October 10, 2019
Published: October 10, 2019

DOI: 10.1021/acsami.9b15349
ACS Appl. Mater. Interfaces 2019, 11, 40944−40950

Scheme 1. Scheme of Individual Au@Ag Nanocube-Based Plasmonic Biosensor

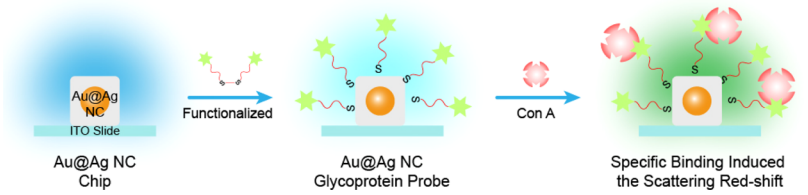

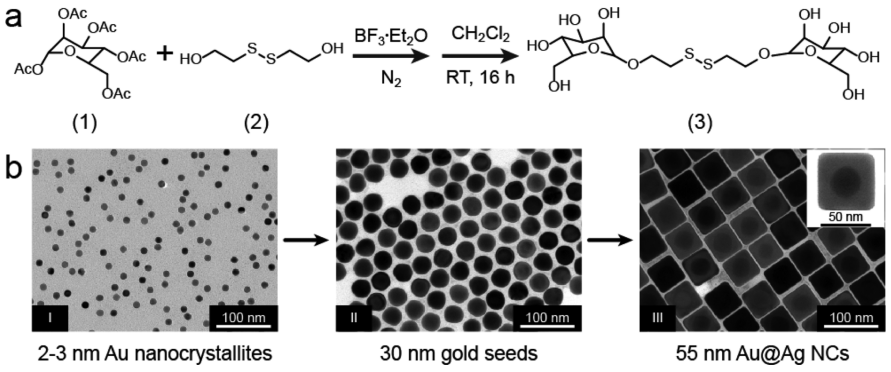

Figure 1. (a) Synthesis route of thiolated D-mannose. (1) 1,2,3,4,6-peracetylated mannose, (2) bis(2-hydroxyethyl) disulfide, and (3) thiolated D-mannose. (b) TEM of 2−3 nm Au nanocrystallites, 30 nm gold seeds, and Au@Ag NCs.

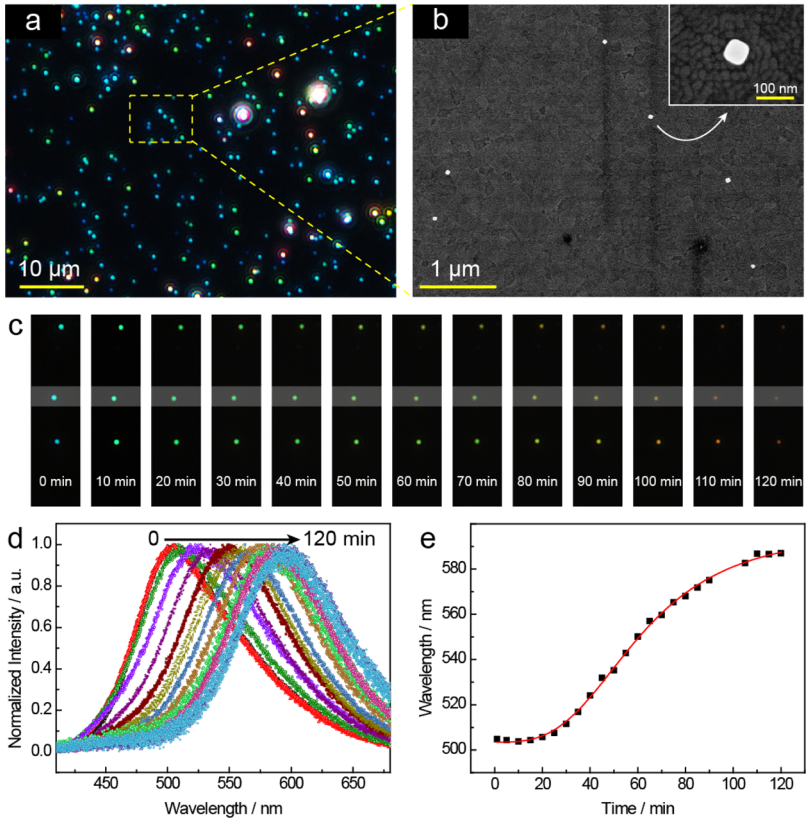

Figure 2. (a) Typical DFM scattering images of Au@Ag NCs; (b) in situ SEM images of ROI (region of interest) in the DFM image; (c) color change with time in the immobilization of mannose on the Au@Ag NC surface by adding 1 mM thiolated D-mannose; (d) typical LSPR spectra of the corresponding single Au@Ag NC surface modification process (0−120 min) in the presence of 1 mM thiolated D-mannose; and (e) LSPR scattering peak position of a selected time-dependent Au@Ag NC (λ_{max}) red shift during mannose molecule modification.

optical sensors or contrast probes in biomedical applications, which provided alternative research methods in catalysis, photonics, and data storage.[35−42] In our previous report, Au@Ag NCs were employed for developing a smart plasmonic nanobiosensor with a single Au@Ag NC. Because of the high sensitivity to the RI change around the Au@AgNCs, the nanobiosensor not only could be used for monitoring the dynamic process of DNA-specific hybridization with the target

DOI: 10.1021/acsami.9b15349
ACS Appl. Mater. Interfaces 2019, 11, 40944−40950

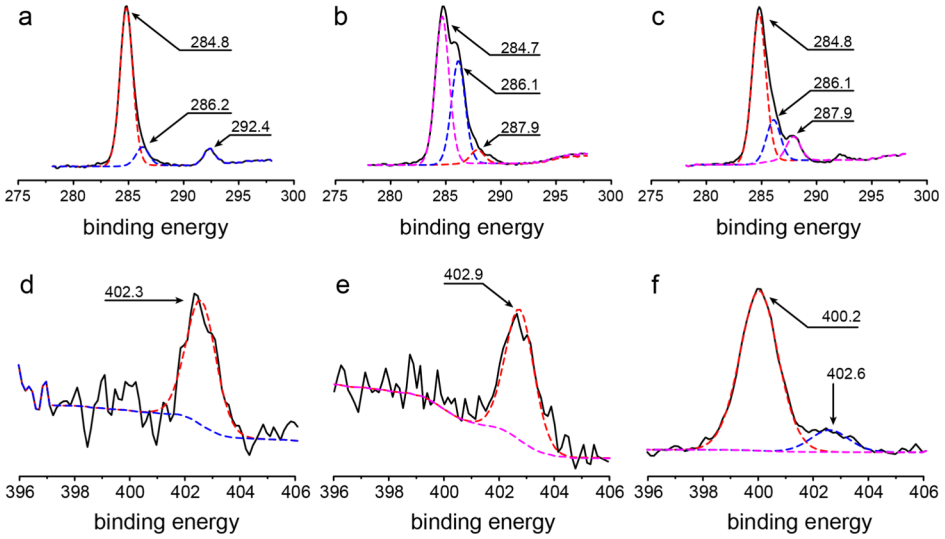

Figure 3. Deconvolution of the C_{1s} (a–c) and N_{1s} (d–f) XPS spectra of Au@Ag NC, Au@Ag@mannose, and Au@Ag@mannose–ConA. Solid line: experimental data; dashed line: fitting curve.

miRNA at a single-molecule level but also enables enzymatic DNA-based logic operations and biomemory cells.[43]

Herein, we present for the first time real-time monitoring of lectin–sugar interactions with a single Au@Ag NC by its LSPR scattering spectra, which could be designed for plasmonic nanobiosensors for trace concanavalin A (ConA) analysis with high sensitivity and selectivity. As shown in Scheme 1, Au@Ag NCs were immobilized on an indium tin oxide (ITO) slide, and then thiolated D-mannose molecules were modified on the surface of Au@Ag NCs by the strong Ag–S bonds. The LSPR scattering spectra of this plasmonic nanobiosensor would red-shift to a long wavelength in the presence of different concentrations of ConA. Furthermore, our studies demonstrated the perfect biosensing ability with the dual channel of dark-field microscopy (DFM) images and scattering spectra, and the results could be certified by X-ray photoelectron spectroscopy (XPS) spectra and in situ scanning electron microscopy (SEM) methods.

2. EXPERIMENTAL METHODS

The compound thiolated D-mannose was synthesized by Flitsch's method[44] (Figure 1a). Typically, D-mannose protected by acetic acid was dissolved in pyridine and acetic anhydride, kept stirring for the reaction overnight at room temperature in vacuum, and then the residue was dissolved in ethyl acetate and washed successively with $NaHCO_3$ and NaCl for hydrolysis of the acetic acid group (details of experimental procedures and corresponding characterization are shown in the Supporting Information). The final products could be used without further purification.

For the preparation of the plasmonic substrate (monodisperse 55 nm Au@Ag core–shell NCs) for fabricating optical plasmonic nanobiosensors, the seed-mediated growth method reported by Xia[28] was employed (Figure 1b). The core–shell substructure of Au@Ag NCs could be easily observed in the transmission electron microscopy (TEM) image and the magnified TEM image (Figure 1b-III) in the insert. The Ag shell was uniformly deposited on the Au seeds, forming a complete coating. Further, there was a clear boundary that could be observed between the Au core and the Ag shell because of the difference in atomic number and thus attenuation of electrons. The edge length was close to that of the calculated results based on the addition of the amount of Au seeds and $AgNO_3$.

3. RESULTS AND DISCUSSION

Because of the good transparency, conductivity, and physical adsorption capacity of ITO, it could not only be used as a plasmonic biochip substrate but also for capturing in situ SEM images without the spraying treatment procedure. The ITO slides were cleaned in an ultrasonic bath for 30 min by using detergent, acetone, ethanol, and water in turn. Diluted Au@Ag NC solution was added on the ITO slides for a short time (1 min) to immobilize Au@Ag NCs onto the ITO slide surface by physical absorption, so that a certain distance about 10–20 μm could be maintained between Au@Ag NCs for distinguishing each nanoparticle in the DFM images. Figure 2a shows a typical DFM image, in which the single Au@Ag NC correspondingly presented as a blue light spot. In addition, the in situ SEM image of the as-prepared plasmonic biochip further proved that the particular size of Au@Ag NC with a detailed view was 55 nm. With the presence of 1.0 mM thiolated D-mannose, the disulfide bond was broken and linked to the Au@Ag NC surface, and this modification process could be monitored real-time not only by the peak position (λ_{max}) of the LSPR scattering spectra on an individual Au@Ag NC (initial λ_{max} located at 508 nm, Figure 2d) but also by the color changing continually form blue to cyan and dark orange (Figure 2c) in the DFM images. Over time, the LSPR scattering intensity of Au@AgNCs went lower and lower because of the limited detection sensitivity of the instrument; 60 min modification became the best choice for preparing these plasmonic nanobiosensors. There was no change in the shape of the Au@Ag NC in situ SEM images after the modification process, and the TEM images of the Au@Ag@mannose nanobiosensor colloid solution provide the same conclusion in the surface modification process and analysis application (Figure S6), indicating that the LSPR scattering spectra shift is mainly dependent on the RI change of the microenvironment surrounding Au@Ag NCs.

As shown in Scheme 1, the Au@Ag NC immobilization on the ITO slide (step 1), functionalization by mannose molecules (step 2), and specific binding between mannose and the target molecules ConA (step 3) were assayed by XPS. The high-resolution XPS spectra for C_{1s} and N_{1s} of Au@Ag NC, Au@Ag@mannose, and Au@Ag@mannose–ConA are

DOI: 10.1021/acsami.9b15349
ACS Appl. Mater. Interfaces 2019, 11, 40944–40950

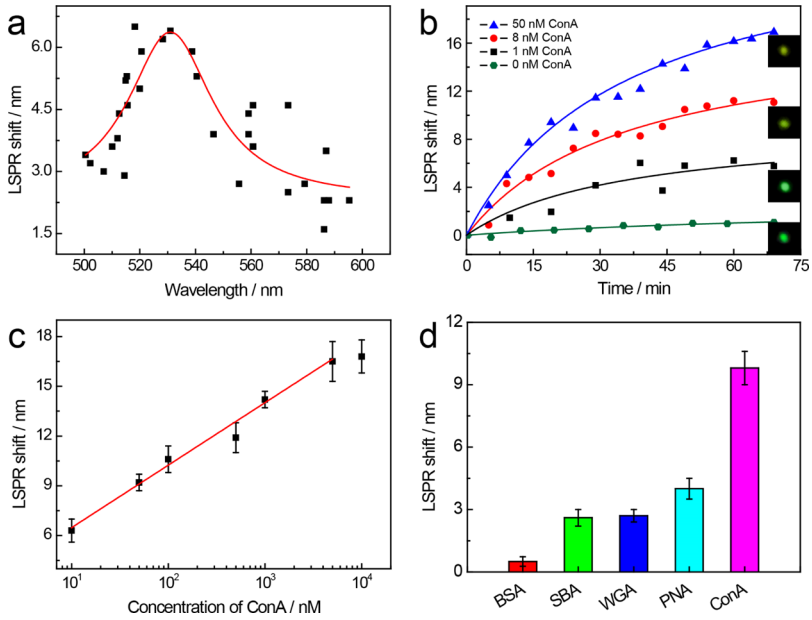

Figure 4. (a) Peak shift with different initial λ_{max}; insert: schematic model of the mannose-substituted surface. (b) Selected Au@Ag@mannose nanobiosensor red shift in different concentrations of ConA [(a−d) 0, 1, 8, and 50 nM]; inset: DFM color images of a typical Au@Ag@mannose nanobiosensor incubated for 60 min in the corresponding ConA solution; (c) line relationship between $\Delta\lambda$ and ConA concentration, $N = 30$; (d) scattering peak shift of Au@Ag@mannose nanobiosensors in BSA, PNA, WGA, SBA, and ConA; $N = 30$.

shown in Figure 3. After the Shirley background correction, the C_{1s} and N_{1s} spectra could be good-fitted by applying the mixed Gaussian/Lorentzian function.

The C_{1s} XPS spectra could be deconvoluted into three components corresponding to the carbon atoms in different functional groups, including the nonoxygenated C (~284.8 eV), the carbon in C−N (~286.1 eV), and the carbonyl carbon (C═O, ~287.9 eV). There were two C_{1s} chemical shifts located at ~284.8 and ~286.2 eV, which were caused by the cetyltrimethylammonium chloride (CTAC) molecules coated on the Au@Ag NC surface. In addition, there appeared a new chemical shift located at 287.9 eV in step 2 that might contribute to the substitution of mannose in place of CTAC. After the specific binding between ConA and mannose molecules, the component was notably decreased for the carbon in C−N (from 34.80 to 19.11%) and increased for carbonyl carbon (from 13.24 to 16.60%).

Before and after the modification of thiolated D-mannose molecules, there was a N_{1s} chemical shift that appeared at ~402.0 eV which was attributed to the contributions from the residual NH_4^+ group on the Au@Ag NC surface. During the specific binding of ConA with the probe molecules, there was a notable N_{1s} chemical shift that appeared at 400.2 eV which was attributed to the high amino acid content. The assignment of peaks in the N_{1s} spectra could further confirm the conclusions of the previous analysis of the C_{1s} components. More than this, the extinction spectra of the Au@Ag@mannose nanobiosensors had successfully verified that Au@Ag@mannose nanobiosensors could directly bind to ConA (Figure S4).

Single-nanoparticle-based LSPR nanobiosensor-enabled sensitive detection with clear spatial resolution had been reported in previous researches,[45,46] but the sensitivity of the amount of the red shift ($\Delta\lambda_{max}$) of the LSPR scattering spectra depended strictly on the differences of the local electromagnetic distribution in the nanoparticles with different sizes and shapes. The $\Delta\lambda_{max}$ values of individual Au@Ag@mannose LSPR scattering spectra were governed by the edge length and the rounded radius of Au@AgNCs. Although it was difficult to control the Au@AgNCs to be in same shape and size in the synthesis process, $\Delta\lambda_{max}$ reaches the maximum and then decreases with the increasing initial λ_{max} under a fixed ConA concentration. Hence, the size of Au@Ag NCs must be selected carefully (with the same initial λ_{max}) to obtain a sufficient intensity of the LSPR scattering signal. When Au@Ag@mannose was employed for the detection of ConA, we found that the LSPR scattering spectra of all Au@Ag@mannose nanobiosensors on the plasmonic biochip showed varying red shifts (Figure 4a) in the same concentration of ConA. The statistical results of a number of nanobiosensors revealed that the initial λ_{max} located at around 528 nm was significantly shifted after specific binding with the same concentration of ConA. These results were similar with those of the previous report by Kiessling and Corn.[47] Further, the reason could be attributed to the lower coverage density of mannose molecules on Au@AgNCs with blue scattering that would lead fewer ConA to bind to the Au@Ag@mannose nanobiosensor, which limited the detection sensitivity of the nanobiosensor. However, for the Au@Ag@mannose nanobiosensor with red scattering, it mainly depended on the larger size of Au@AgNCs, which led to a lower mannose coverage after the same modification process and then fewer ConA binding to the nanosensor. The amount of ConA binding on Au@Ag@mannose would limit the interfacial reaction because of steric hindrance.[31] For this reason, the result indicated that the best modification time is 60 min, and the Au@Ag@mannose nanobiosensor exhibited that its LSPR scattering spectral peak position was located around 528 nm. According to the previous report about the small-molecule adsorbates on AgNPs by Van Duyne[45,48] and the linear relation between the surface coverage and LSPR spectral red shift,[31] we could conjecture that there were fewer than 3000 mannose molecules on every Au@Ag NC.

Similar with the modification procedure in Figure 2d, λ_{max} of the LSPR spectra of single Au@Ag nanobiosensors exhibited

DOI: 10.1021/acsami.9b15349
ACS Appl. Mater. Interfaces 2019, 11, 40944−40950

higher sensitivity than that in colloid solution (Figure S5) and continually shifted to a longer wavelength by the treatment of ConA at different times. With the increasing ConA concentration, the plasmonic nanobiosensor exhibited a dual-channel sensing ability of the red-shift phenomenon of different LSPR scattering spectra, and the color changed from green to yellowish green (Figure 4b). The $\Delta\lambda_{max}$ value quickly reached the maximum value at a higher concentration of ConA, which suggested a higher collision and binding probability between ConA and D-mannose. To evaluate the sensitivity of this nanobiosensor system, testing on $\Delta\lambda_{max}$ at different ConA concentrations was performed in the range of 10 nM to 10 μM. As shown in Figure 4c, $\Delta\lambda_{max}$ of the Au@Ag@mannose nanobiosensors increased with the increasing concentrations of ConA until it was saturated. Accordingly, this sensing system could be used for the analysis of target proteins in a large range, with a linear relation between $\Delta\lambda_{max}$ and the ConA concentration (C_{ConA}), and the results were fitted by a regression equation which is expressed as $\Delta\lambda = 0.057 \times \log C_{ConA} + 0.026$ ($R^2 = 0.97$). The successful analysis of ConA by $\Delta\lambda_{max}$ of the LSPR scattering spectra of Au@Ag@mannose nanobiosensors provided evidence for the following specific binding process. One time of peanut agglutinin (PNA), wheat germ agglutinin (WGA), soybean agglutinin (SBA) and 10 times of bovine serum albumin (BSA) were used as interference factors for the analysis of the selectivity of plasmonic nanobiosensors. Compared with the presence of ConA, there was no notable red shift with the BSA-containing solution. Although the scattering spectra of all the Au@Ag@mannose nanobiosensors were red-shifted to various lower degrees with PNA, WGA, and SBA, these results could still be used for distinguishing the interference protein. As shown in Figure 4d, there was a significant distinction in $\Delta\lambda_{max}$ of the Au@Ag@mannose nanobiosensors with or without interference.

4. CONCLUSIONS

In summary, we exhibited a novel plasmonic nanobiosensor for the detection of ConA or real time, following the specific binding process of lectin−sugar interactions on a single Au@Ag NC, which enables the miniaturization of the biosensor system to nanoscale. The LSPR spectra of the Au@Ag NCs were linearly red-shifted as the concentration of ConA increased (10 nM to 10 μM), and the limit of detection of these plasmonic nanobiosensors was as low as 2 nM. Furthermore, the results demonstrated the perfect biosensing ability with the dual channel of DFM images and LSPR spectra. We believe that this nanobiosensor system can provide an alternative important method for monitoring the lectin−sugar specific binding at a single nanoparticle surface. Accordingly, future efforts will be focused on to characterize other specific binding processes using single plasmonic nanoparticles in vitro.

■ ASSOCIATED CONTENT

Supporting Information

The Supporting Information is available free of charge on the ACS Publications website at DOI: 10.1021/acsami.9b15349.

Sequences of the nucleic acids, UV−vis spectral SEM and TEM images of 55 nm AgNCs, and additional experiments relating to assembling (PDF)

■ AUTHOR INFORMATION

Corresponding Authors

*E-mail: iamlzhang@njupt.edu.cn (L.Z.).
*E-mail: iamqlfan@njupt.edu.cn (Q.F.).
*E-mail: wbwu@njfu.edu.cn (W.W.).
*E-mail: iamwhuang@njupt.edu.cn (W.H.).

ORCID

Lei Zhang: 0000-0002-0045-2539
Quli Fan: 0000-0002-9387-0165
Shufen Chen: 0000-0003-0333-958X
Weibing Wu: 0000-0003-2786-9585
Lianhui Wang: 0000-0001-9030-9172
Wei Huang: 0000-0001-7004-6408

Author Contributions

J.S. and L.Z. contributed equally to this work. The manuscript was written through contributions of all authors. All authors have given approval to the final version of the manuscript.

Notes

The authors declare no competing financial interest.

■ ACKNOWLEDGMENTS

For the financial support for this work, we thank the National Natural Science Foundation of China (nos. 61571239, 21674048, and 21574064), the Jiangsu Province "333 high-level Personnel Training project", the Primary Research &Development Plan of Jiangsu Province (BE2016770), and the Natural Science Foundation of Jiangsu Province of China (nos. BK20171020, NY218033).

■ ABBREVIATIONS

ConA, concanavalin A
PNA, peanut agglutinin
WGA, wheat germ agglutinin
SBA, soybean agglutinin
BSA, albumin from bovine serum
DFM, dark-field microscopy
RI, reflective index
NC, nanocube
LSPR, localized surface plasmon resonance
ITO, indium tin oxide

■ REFERENCES

(1) Gabius, H.; Andre, S.; Kaltner, H.; Siebert, H. C. The Sugar Code: Functional Lectinomics. *Biochim. Biophys. Acta* **2002**, *1572*, 165−177.

(2) Li, W.; Yu, R.; Ma, B.; Yang, Y.; Jiao, X.; Liu, Y.; Cao, H.; Dong, W.; Liu, L.; Ma, K.; Fukuda, T.; Liu, Q.; Ma, T.; Wang, Z.; Gu, J.; Zhang, J.; Taniguchi, N. Core Fucosylation of Igg B Cell Receptor Is Required For Antigen Recognition and Antibody Production. *J. Immunol.* **2015**, *194*, 2596−2606.

(3) Dewald, J. H.; Colomb, F.; Bobowski-Gerard, M.; Groux-Degroote, S.; Delannoy, P. Role of Cytokine-Induced Glycosylation Changes in Regulating Cell Interactions and Cell Signaling in Inflammatory Diseases and Cancer. *Cells* **2016**, *5*, 43.

(4) Cagnoni, A. J.; Perez Saez, J. M.; Rabinovich, G. A.; Marino, K. V. Turning-Off Signaling by Siglecs, Selectins, and Galectins: Chemical Inhibition of Glycan-Dependent Interactions in Cancer. *Front. Oncol.* **2016**, *6*, 109.

(5) Oliveira-Ferrer, L.; Legler, K.; Milde-Langosch, K. Role of Protein Glycosylation in Cancer Metastasis. *Semin. Cancer Biol.* **2017**, *44*, 141−152.

(6) Jelinek, R.; Kolusheva, S. Carbohydrate Biosensors. *Chem. Rev.* **2004**, *104*, 5987−6016.

DOI: 10.1021/acsami.9b15349
ACS Appl. Mater. Interfaces 2019, 11, 40944−40950

(7) Reichardt, N. C.; Martín-Lomas, M.; Penadés, S. Glyconanotechnology. *Chem. Soc. Rev.* **2013**, *42*, 4358−4376.
(8) Munoz, E. M.; Correa, J.; Riguera, R.; Fernandez-Megia, E. Real-Time Evaluation of Binding Mechanisms in Multivalent Interactions: A Surface Plasmon Resonance Kinetic Approach. *J. Am. Chem. Soc.* **2013**, *135*, 5966−5969.
(9) Xiong, B.; Zhou, R.; Hao, J.; Jia, Y.; He, Y.; Yeung, E. S. Highly Sensitive Sulphide Mapping in Live Cells By Kinetic Spectral Analysis of Single Au-Ag Core-Shell Nanoparticles. *Nat. Commun.* **2013**, *4*, 1708.
(10) Hao, J.; Xiong, B.; Cheng, X.; He, Y.; Yeung, E. S. High-Throughput Sulfide Sensing With Colorimetric Analysis of Single Au-Ag Core-Shell Nanoparticles. *Anal. Chem.* **2014**, *86*, 4663−4667.
(11) Zhang, L.; Li, Y.; Li, D.-W.; Jing, C.; Chen, X.; Lv, M.; Huang, Q.; Long, Y.-T.; Willner, I. Single Gold Nanoparticles as Real-Time Optical Probes for the Detection of NADH-Dependent Intracellular Metabolic Enzymatic Pathways. *Angew. Chem., Int. Ed.* **2011**, *50*, 6789−6792.
(12) Maalouli, N.; Barras, A.; Siriwardena, A.; Bouazaoui, M.; Boukherroub, R.; Szunerits, S. Comparison of Photo- and Cu(I)-Catalyzed "Click" Chemistries for the Formation of Carbohydrate SPR Interfaces. *Analyst* **2013**, *138*, 805−812.
(13) Wang, W.; Soriano, B.; Chen, Q. Glycan Profiling of Proteins Using Lectin Binding By Surface Plasmon Resonance. *Anal. Biochem.* **2017**, *538*, 53−63.
(14) Shi, L.; Jing, C.; Ma, W.; Li, D.-W.; Halls, J. E.; Marken, F.; Long, Y.-T. Plasmon Resonance Scattering Spectroscopy at the Single-Nanoparticle Level: Real-Time Monitoring of A Click Reaction. *Angew. Chem., Int. Ed.* **2013**, *52*, 6011−6014.
(15) Choi, Y.; Park, Y.; Kang, T.; Lee, L. P. Selective and Sensitive Detection of Metal Ions By Plasmonic Resonance Energy Transfer-Based Nanospectroscopy. *Nat. Nanotechnol.* **2009**, *4*, 742−746.
(16) Jing, C.; Shi, L.; Liu, X.; Long, Y.-T. A Single Gold Nanorod as A Plasmon Resonance Energy Transfer Based Nanosensor for High-Sensitivity Cu(II) Detection. *Analyst* **2014**, *139*, 6435−6439.
(17) Ajay Piriya, V. S.; Joseph, P.; Kiruba Daniel, S. C. G.; Lakshmanan, S.; Kinoshita, T.; Muthusamy, S. Colorimetric Sensors for Rapid Detection of Various Analytes. *Mater. Sci. Eng., C* **2017**, *78*, 1231−1245.
(18) Novo, C.; Funston, A. M.; Mulvaney, P. Direct Observation of Chemical Reactions on Single Gold Nanocrystals Using Surface Plasmon Spectroscopy. *Nat. Nanotechnol.* **2008**, *3*, 598−602.
(19) Minamimoto, H.; Toda, T.; Futashima, R.; Li, X.; Suzuki, K.; Yasuda, S.; Murakoshi, K. Visualization of Active Sites for Plasmon-Induced Electron Transfer Reactions Using Photoelectrochemical Polymerization of Pyrrole. *J. Phys. Chem. C* **2016**, *120*, 16051−16058.
(20) Song, H.; Meng, X.; Dao, T. D.; Zhou, W.; Liu, H.; Shi, L.; Zhang, H.; Nagao, T.; Kako, T.; Ye, J. Light-Enhanced Carbon Dioxide Activation and Conversion by Effective Plasmonic Coupling Effect of Pt and Au Nanoparticles. *ACS Appl. Mater. Interfaces* **2018**, *10*, 408−416.
(21) Wu, D.-Y.; Zhang, M.; Zhao, L.-B.; Huang, Y.-F.; Ren, B.; Tian, Z.-Q. Surface Plasmon-Enhanced Photochemical Reactions on Noble Metal Nanostructures. *Sci. China Chem.* **2015**, *58*, 574−585.
(22) Shen, Y.; Zhou, J.; Liu, T.; Tao, Y.; Jiang, R.; Liu, M.; Xiao, G.; Zhu, J.; Zhou, Z.-K.; Wang, X.; Jin, C.; Wang, J. Plasmonic Gold Mushroom Arrays With Refractive Index Sensing Figures of Merit Approaching the Theoretical Limit. *Nat. Commun.* **2013**, *4*, 2381.
(23) Mock, J. J.; Smith, D. R.; Schultz, S. Local Refractive Index Dependence of Plasmon Resonance Spectra from Individual Nanoparticles. *Nano Lett.* **2003**, *3*, 485−491.
(24) Chen, J.; Shi, S.; Su, R.; Qi, W.; Huang, R.; Wang, M.; Wang, L.; He, Z. Optimization and Application of Reflective LSPR Optical Fiber Biosensors Based on Silver Nanoparticles. *Sensors* **2015**, *15*, 12205−12217.
(25) Ribaut, C.; Voisin, V.; Malachovská, V.; Dubois, V.; Mégret, P.; Wattiez, R.; Caucheteur, C. Small Biomolecule Immunosensing With Plasmonic Optical Fiber Grating Sensor. *Biosens. Bioelectron.* **2016**, *77*, 315−322.
(26) Wang, Q.; Liu, R.; Yang, X.; Wang, K.; Zhu, J.; He, L.; Li, Q. Surface Plasmon Resonance Biosensor for Enzyme-Free Amplified Microrna Detection Based on Gold Nanoparticles and DNA Supersandwich. *Sens. Actuators, B* **2016**, *223*, 613−620.
(27) Tian, Y.; Zhang, L.; Shen, J.; Wu, L.; He, H.; Ma, D.-L.; Leung, C.-H.; Wu, W.; Fan, Q.; Huang, W.; Wang, L. An Individual Nanocube-Based Plasmonic Biosensor for Real-Time Monitoring the Structural Switch of the Telomeric G-Quadruplex. *Small* **2016**, *12*, 2913−2920.
(28) Ma, Y.; Li, W.; Cho, E. C.; Li, Z.; Yu, T.; Zeng, J.; Xie, Z.; Xia, Y. Au@Ag Core-Shell Nanocubes With Finely Tuned and Well-Controlled Sizes, Shell Thicknesses, and Optical Properties. *ACS Nano* **2010**, *4*, 6725−6734.
(29) Hu, Y.; Zhang, L.; Zhang, Y.; Wang, B.; Wang, Y.; Fan, Q.; Huang, W.; Wang, L. Plasmonic Nanobiosensor Based on Hairpin DNA for Detection of Trace Oligonucleotides Biomarker in Cancers. *ACS Appl. Mater. Interfaces* **2015**, *7*, 2459−2466.
(30) Zhang, L.; Wang, J.; Zhang, J.; Liu, Y.; Wu, L.; Shen, J.; Zhang, Y.; Hu, Y.; Fan, Q.; Huang, W.; Wang, L. Individual Au-Nanocube Based Plasmonic Nanoprobe for Cancer Relevant MicroRNA Biomarker Detection. *ACS Sens.* **2017**, *2*, 1435−1440.
(31) Zhang, L.; Zhang, Y.; Hu, Y.; Fan, Q.; Yang, W.; Li, A.; Li, S.; Huang, W.; Wang, L. Refractive Index Dependent Real-Time Plasmonic Nanoprobes on Single Silver Nanocube for Ultrasensitive Detection of the Lung Cancer-Associated Mirnas. *Chem. Commun.* **2015**, *51*, 294−297.
(32) Ao, H.; Qian, Z.; Zhu, Y.; Zhao, M.; Tang, C.; Huang, Y.; Feng, H.; Wang, A. A Fluorometric Biosensor Based on Functional Au/Ag Nanoclusters for Real-Time Monitoring of Tyrosinase Activity. *Biosens. Bioelectron.* **2016**, *86*, 542−547.
(33) Tang, L.; Li, S.; Han, F.; Liu, L.; Xu, L.; Ma, W.; Kuang, H.; Li, A.; Wang, L.; Xu, C. SERS-Active Au@Ag Nanorod Dimers for Ultrasensitive Dopamine Detection. *Biosens. Bioelectron.* **2015**, *71*, 7−12.
(34) Song, L.; Mao, K.; Zhou, X.; Hu, J. A novel biosensor based on Au@Ag Core-Shell Nanoparticles for SERS Detection of Arsenic (III). *Talanta* **2016**, *146*, 285−290.
(35) Zhang, Q.; Li, N.; Goebl, J.; Lu, Z.; Yin, Y. A Systematic Study of the Synthesis of Silver Nanoplates: Is Citrate A "Magic" Reagent? *J. Am. Chem. Soc.* **2011**, *133*, 18931−18939.
(36) Xiong, Y.; Washio, I.; Chen, J.; Sadilek, M.; Xia, Y. Trimeric Clusters of Silver in Aqueous $AgNO_3$ Solutions and Their Role as Nuclei in Forming Triangular Nanoplates of Silver. *Angew. Chem., Int. Ed.* **2007**, *46*, 4917−4921.
(37) Zeng, J.; Tao, J.; Su, D.; Zhu, Y.; Qin, D.; Xia, Y. Selective Sulfuration at the Corner Sites of A Silver Nanocrystal and Its Use in Stabilization of the Shape. *Nano Lett.* **2011**, *11*, 3010−3015.
(38) Sun, Y.; Xia, Y. Triangular Nanoplates of Silver: Synthesis, Characterization, and Use as Sacrificial Templates for Generating Triangular Nanorings of Gold. *Adv. Mater.* **2003**, *15*, 695−699.
(39) Kim, T.; Zhang, Q.; Li, J.; Zhang, L.; Jokerst, J. V. A Gold/Silver Hybrid Nanoparticle for Treatment and Photoacoustic Imaging of Bacterial Infection. *ACS Nano* **2018**, *12*, 5615−5625.
(40) Liu, Y.; Zhou, J.; Wang, B.; Jiang, T.; Ho, H.-P.; Petti, L.; Mormile, P. Au@Ag Core-Shell Nanocubes: Epitaxial Growth Synthesis and Surface-Enhanced Raman Scattering Performance. *Phys. Chem. Chem. Phys.* **2015**, *17*, 6819−6826.
(41) Yuan, P.; Ma, R.; Gao, N.; Garai, M.; Xu, Q.-H. Plasmon Coupling-Enhanced Two-Photon Photoluminescence of Au@Ag Core-Shell Nanoparticles and Applications in the Nuclease Assay. *Nanoscale* **2015**, *7*, 10233−10239.
(42) Hatef, A.; Darvish, B.; Dagallier, A.; Davletshin, Y. R.; Johnston, W.; Kumaradas, J. C.; Rioux, D.; Meunier, M. Analysis of Photoacoustic Response from Gold-Silver Alloy Nanoparticles Irradiated by Short Pulsed Laser in Water. *J. Phys. Chem. C* **2015**, *119*, 24075−24080.
(43) Zhang, Y.; Shuai, Z.; Zhou, H.; Luo, Z.; Liu, B.; Zhang, Y.; Zhang, L.; Chen, S.; Chao, J.; Weng, L.; Fan, Q.; Fan, C.; Huang, W.; Wang, L. Single-Molecule Analysis of Microrna and Logic Operations

DOI: 10.1021/acsami.9b15349
ACS Appl. Mater. Interfaces 2019, 11, 40944−40950

Using A Smart Plasmonic Nanobiosensor. *J. Am. Chem. Soc.* **2018**, *140*, 3988−3993.
(44) Šardzík, R.; Noble, G. T.; Weissenborn, M. J.; Martin, A.; Webb, S. J.; Flitsch, S. L. Preparation of Aminoethyl Glycosides for Glycoconjugation. *Beilstein J. Org. Chem.* **2010**, *6*, 699−703.
(45) McFarland, A. D.; Van Duyne, R. P. Single Silver Nanoparticles as Real-Time Optical Sensors With Zeptomole Sensitivity. *Nano Lett.* **2003**, *3*, 1057−1062.
(46) Eah, S.-K.; Jaeger, H. M.; Scherer, N. F.; Wiederrecht, G. P.; Lin, X.-M. Plasmon Scattering From A Single Gold Nanoparticle Collected Through An Optical Fiber. *Appl. Phys. Lett.* **2005**, *86*, 031902.
(47) Smith, E. A.; Thomas, W. D.; Kiessling, L. L.; Corn, R. M. Surface Plasmon Resonance Imaging Studies of Protein-Carbohydrate Interactions. *J. Am. Chem. Soc.* **2003**, *125*, 6140−6148.
(48) Malinsky, M. D.; Kelly, K. L.; Schatz, G. C.; Van Duyne, R. P. Chain Length Dependence and Sensing Capabilities of the Localized Surface Plasmon Resonance of Silver Nanoparticles Chemically Modified with Alkanethiol Self-Assembled Monolayers. *J. Am. Chem. Soc.* **2001**, *123*, 1471−1482.

DOI: 10.1021/acsami.9b15349
ACS Appl. Mater. Interfaces 2019, 11, 40944−40950